



Research Paper

Fabrication of InVO₄/AgVO₃ heterojunctions with enhanced photocatalytic antifouling efficiency under visible-light

Xin Zhang^a, Jie Zhang^{a,*}, Jianqiang Yu^{b,*}, Yan Zhang^b, Zhaoxia Cui^a, Yan Sun^a, Baorong Hou^a

^a Key Laboratory of Marine Environmental Corrosion and Bio-fouling, Institute of Oceanology, Chinese Academy of Sciences, Qingdao 266071, Shandong, China

^b School of Chemistry and Chemical Engineering, Qingdao University, Qingdao 266071, China

ARTICLE INFO

Article history:

Received 2 May 2017

Received in revised form 21 July 2017

Accepted 25 July 2017

Available online 3 August 2017

Keywords:

InVO₄/AgVO₃ heterojunction

Photocatalytic antifouling

Charge separation

Photocatalytic performance

ABSTRACT

With the increasing of bacterial resistance to available antibiotics and water contamination by poisonous organic dyes, it's necessary to consider how to overcome these concerns. In this paper, novel visible-light-sensitive InVO₄/AgVO₃ photocatalysts with a *p-n* junction were synthesized through an ion exchange and in-situ growth process. The obtained photocatalysts were characterized by X-ray powder diffraction (XRD), Transmission electron microscopy (TEM), field-emission scanning electron microscopy (FE-SEM), energy-dispersive X-ray spectroscopy (EDS), high resolution transmission electron microscopy (HRTEM), X-ray photoelectron spectroscopy (XPS) and UV-vis diffuse reflectance spectroscopy (UV-DRS) respectively. It can be observed that the AgVO₃ exhibits a rod-shaped structure, while a plentiful of spherical shaped InVO₄ particles are formed on the surface. The rod-shaped structure of AgVO₃ wasn't changed by the addition of InVO₄, but its photocatalytic properties were tremendously improved. The best photocatalyst was 0.5InVO₄/AgVO₃, over which the Rhodamine B (RhB) solution was almost decomposed in 200 min under visible light irradiation. Moreover, about 99.999% of *P. aeruginosa* (*P. aeruginosa*) (*P. aeruginosa*), *Escherichia coli* (*E. coli*) and *Staphylococcus aureus* (*S. aureus*) were killed over 0.5InVO₄/AgVO₃ at 30 min. From these results it can be inferred that 0.5InVO₄/AgVO₃ heterojunctional photocatalyst has an improved efficiency for the separation of the current carriers to enhance the photocatalytic performances. This result provided a valuable design for the novel InVO₄/AgVO₃ heterojunction photocatalysts with excellent photocatalytic properties used in marine antifouling.

© 2017 Elsevier B.V. All rights reserved.

1. Introduction

With the development of marine exploration, there has been a growing attention on the issue of marine biofouling all over the world, which resulted into enormous economic losses and serious security incidents to ocean development [1]. In order to reduce the harm of biofouling, antifouling coating is one of the most effective uses on the surface technology, but this technique triggered serious drug resistance owing to their high biotoxicity [2]. Nowadays, however, resistance to antibiotics and other antibacterial material had been reaching a dangerous level which invalidating the existing antimicrobial drugs. Therefore, it is essential to exploit environmentally friendly antifouling materials to substitute the toxic materials.

In the last few years, a novel and green photocatalytic technology based on semiconductors has been widely concerned, which can harness solar irradiation as a source of energy and show promising applications in the degradation of pollutants, splitting of water and sterilization [3–8]. At the present time, developing visible-light-responsive photocatalysts is the most important matter in this field, because the utilization of visible light, which accounts for more than half of the solar spectrum, is significant. Among all the visible light-driven photocatalysts with narrow band-gap examined so far, metal vanadate photocatalysts (MVO₄ where M = Ag, Bi, Al, Ti, In, Fe, Sr, etc.) have been widely investigated and applied in many fields of sciences and industrial [9–13].

Indium vanadate (InVO₄), with a bandgap of 2.0 eV, is one of these visible-light responsive metal vanadate photocatalysts and has received extensive interest owing to its various applications in many fields, including degradation of air purification, water splitting, organic pollutants, and so on [14–19].

* Corresponding authors.

E-mail addresses: zhangjie@qdio.ac.cn (J. Zhang), jianqyu@qdu.edu.cn (J. Yu).

According to the previous research works [12,20–22], solid phase reaction, hydrothermal and sol-gel synthesis have been applied to synthesizing monoclinic or orthorhombic crystals of InVO₄. Nevertheless, the performance of InVO₄ photocatalyst is not ideal due to its low efficiency on separating photogenerated electron-hole pairs. In addition, the performance of photocatalytic under visible-light irradiation could be improved by synthesized heterojunction photocatalysts with InVO₄, such as TiO₂/InVO₄ [23] and BiVO₄/InVO₄ [24].

Silver vanadates have attracted increasing attention because of their excellent electrical properties and applications [25–29]. The crystalline phase and stoichiometry of such materials, depend heavily upon reaction conditions, intensively affect the functionalities. Silver vanadate has also been used as an efficient photocatalyst for environment purification [30–32]. This silver vanadate is a cheap, stable material that is abundant and has a controllable surface, so it can be treated as a new material for environmental application.

Therefore, in this study, the novel InVO₄/AgVO₃ photocatalysts were prepared for the first time by ion exchange and in-situ growth methods. The obtained photocatalysts were characterized by XRD, FESEM, EDS, HRTEM, XPS and UV-DRS respectively. The photocatalytic activities of InVO₄, AgVO₃, and InVO₄/AgVO₃ heterojunctions were presented by the degradation of RhB solution and the antibacterial activity under visible light irradiation. Moreover, the mechanism for the photocatalytic efficiency enhancement of these photocatalysts was proposed by trapping free radicals experiments and calculating energy band.

2. Experimental section

2.1. Preparation of the photocatalysts

All chemicals were analytical reagent (AR) grade and used without extra treatment. In a typical experiment, AgVO₃ photocatalysts were obtained by a facile hydrothermal method [33]. The typical synthesis process is as follows: 1 mmol AgNO₃ and 1 mmol NH₄VO₃ were respectively dissolved in 30 mL distilled water under magnetic stirring to obtain solution A and B. Subsequently, solution B was slowly added dropwise to solution A under stirring to form a final suspension, then the pH value was adjusted to 7.0 with 25 wt% NH₃·H₂O and 2 mol/L HNO₃. The suspension was stirred for 1 h in dark, and transferred into a 100 mL Teflon-lined autoclave, and followed by treating it at 180 °C for 24 h. After that, the yellow products were cooled to room temperature naturally, and washed for several times with Milli-Q water and absolute ethanol, respectively. Finally, the samples were dried at 60 °C in air for 6 h to obtain the pure AgVO₃ crystals.

The novel InVO₄/AgVO₃ photocatalysts were prepared by ion exchange and in-situ growth method as follows: 1.0 mmol AgVO₃ was dispersed in 30 mL distilled water under magnetic stirring. Then, In(NO₃)₄·4.5H₂O and 0.25 g PVP were added to the above solution and then adjusted pH value to 7.0 with 25 wt% NH₃·H₂O. The obtained solid composites were then calcined at 160 °C for 12 h. After cooling to room temperature naturally, the precipitations were collected, washed for several times and then dried in air at 60 °C. According to this method, InVO₄/AgVO₃ nanocomposites were prepared with various molar ratios of In and Ag, which were denoted as 0.25InVO₄/AgVO₃, 0.5InVO₄/AgVO₃, 0.75InVO₄/AgVO₃, and 1InVO₄/AgVO₃, where the molar ratio of In and Ag was 0.25:1, 0.5:1, 0.75:1 and 1:1, respectively. In addition, the pure InVO₄ and AgVO₃ crystals were also prepared by the same conditions.

2.2. The characterizations of the photocatalysts

The crystalline structures of the samples were characterized by XRD with Rigaku D/max-3CX-ray diffraction operating at 40 kV and 30 mA with Cu K α radiation ($\lambda = 0.15406$ nm). The morphologies were performed by FE-SEM (Hitachi S-4800, Japan) operating at 10 kV. TEM and HRTEM images were implemented on a Tecnai G220 transmission electron microscope at 200 kV acceleration voltage with EDS for elemental analysis. The XPS measurements were measured on Multifunctional imaging electron spectrometer (Thermo ESCALAB 250XI, USA) with total power dissipation of 150 W (15 kV, 10 mA). The UV-vis absorption spectroscopy of the samples were carried out on Hitachi U-4100 UV Spectrometer (Japan) using BaSO₄ as the reference.

2.3. Photocatalytic performance

The photocatalytic activities of the synthesized materials were determined by degradation of RhB under visible light at room temperature. A 800 W xenon lamp was used as the light source, and a cutoff filter was used to remove the wavelength of light less than 420 nm [34]. In those experiments, 25 mg of photocatalysts were dispersed into 50 mL of 50 mg/L RhB solution with quartz tubes respectively. In order to ensure the adsorption/desorption equilibrium, these solution was stirred for 30 min in darkness before irradiation. The photocatalytic degradation ratio was measured by the absorption peak at 553 nm to determine the remnant concentration of RhB at different intervals by the same UV-DRS (UV-2550, Shimadzu, Japan).

Antibacterial response was measured against *E.coli*, *S. aureus* and *P. aeruginosa* which have been pervasively applied to model bacteria in previous research [35–37]. The bacterial stock suspensions concentrations were typically 10⁶ cfu/mL. Then, the photocatalytic antifouling experiments were measured by a 800 W xenon lamp with a cutoff filter. In addition, 25 mg of photocatalyst, 49.5 mL of sterilized natural seawater or PBS, and 500 μ L of bacterial suspension was added into 50 mL of quartz tubes in sequence. After stirred for 30 min in darkness, the suspensions were exposed to light irradiation for another 30 min. 1 mL of the bacteria suspension was fetched and diluted several multiples with sterilized seawater or PBS every 10 min. Besides, 100 μ L of these suspension was immediately coated on LB agar plates and cultured of these bacteria at 37 °C for 24 h to calculated the number of bacteria colony (in cfu). According to the blank control which was disposed without photocatalysts, the antibacterial rate was computed as follows:

$$\text{Antibacteria rate (\%)} = 100 - \left(\frac{N_t}{N_0} \right) \times 100$$

Where, N₀ and N_t are the numbers of bacteria colony in the blank control and the samples with photocatalysts, respectively. Therefore, the anti-microbial rate could be defined as follows:

$$\text{Antimicrobial rate (\%)} = 100 - \text{survial rate}$$

The active free-radicals were trapping by adding scavengers, in which the concentrations of IPA (a scavenger of hydroxyl radical, •OH), of DS (a scavenger of superoxide radical, •O₂⁻), and sodium oxalate (a scavenger of holes, h⁺) were used in solutions with the addition of 1 mmol of quencher [24,38].

3. Results and discussions

3.1. The structural analysis of the photocatalysts

The X-ray diffraction (XRD) patterns of the as-prepared samples are shown in Fig. 1. For pure InVO₄, every diffraction peak

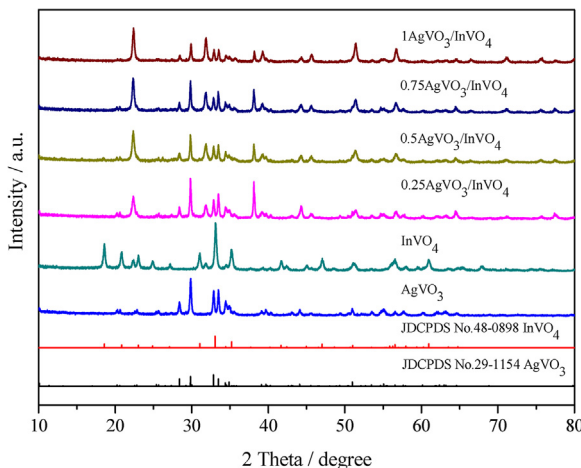


Fig. 1. XRD patterns of as-synthesized samples: AgVO₃, InVO₄ and InVO₄/AgVO₃.

can be indexed to InVO₄ phase, which is also confirmed by the standard data (JCPDS No. 48-0898). And all the peaks of AgVO₃ can be easily indexed into crystal planes of pure AgVO₃ phase (JCPDS No. 29-1154) in the XRD pattern. When overlapping the two semiconductors, the central characteristic diffraction peaks of the heterostructured nanorods did not change greatly. In addition, no other peaks from possible impurities were detected in these XRD patterns. As shown in Fig. 1, the pure InVO₄ sample showed the diffraction peaks at $2\theta = 31.0^\circ, 35.2^\circ, 51.0^\circ, 56.5^\circ$ and 64.7° which can be indexed to the InVO₄ (112), (130), (042), (312) and (400) planes, respectively (JCPDS No: 48-0898) [5]. Moreover, for the AgVO₃ phase, the strong peaks appeared at $22.5^\circ, 28.4^\circ, 29.8^\circ, 32.8^\circ, 45.5^\circ, 50.9^\circ, 55.0^\circ, 55.5^\circ, 56.5^\circ$ and 60.1° , which could be confirmed to the AgVO₃ phase (JCPDS No. 29-1154) for (002), (-211), (501), (-411), (-112), (321), (020), (-514), (512), (-222) and (521) planes [37,39]. The InVO₄/AgVO₃ heterostructure showed a compound of InVO₄ phase (JCPDS No. 48-0898) and AgVO₃ phase (JCPDS No. 29-1154), revealing that the mixture was the main composition of InVO₄/AgVO₃ heterostructure.

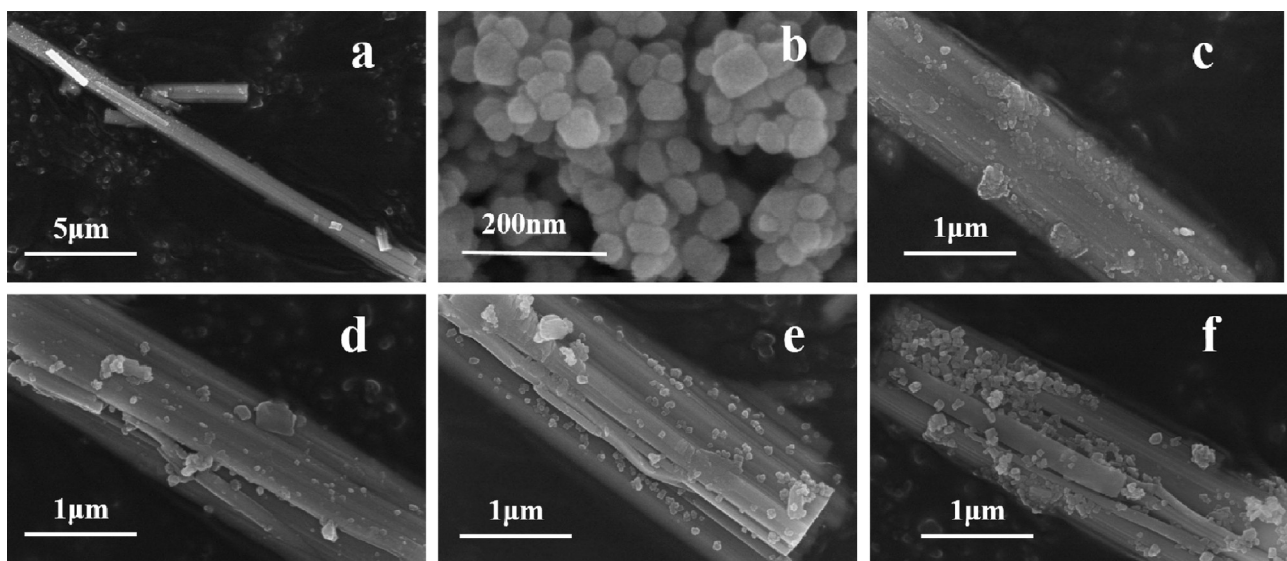


Fig. 2. FESEM images of as-synthesized samples: (a) AgVO₃, (b) InVO₄, (c) 0.25 InVO₄/AgVO₃, (d) 0.5 InVO₄/AgVO₃, (e) 0.75InVO₄/AgVO₃ and (f) 1InVO₄/AgVO₃.

3.2. The morphologies of the photocatalysts

Fig. 2(a-e) shows the FE-SEM images of the as-prepared AgVO₃, InVO₄ and InVO₄/AgVO₃ samples with various molar ratio of In/Ag. As shown in **Fig. 2(a)**, the FE-SEM image of AgVO₃ sample revealed a one-dimensional (1D) rod-like morphology with diameters of about 1 μm. **Fig. 2(b)** showed that the shape of the pure InVO₄ crystals were irregular spherical particles with an average size of 50 nm. As for the InVO₄/AgVO₃ heterostructure, plentiful rod-like structure with spherical shapes can be observed in **Fig. 2(c-f)**. However, these heterostructures were different from each other on account of the different percent of AgVO₃ and InVO₄. Compared to the rod-like structure of pure AgVO₃, the 0.5InVO₄/AgVO₃ composites exhibited favorable nanorod structures with diameters of about 1 μm (**Fig. 2(c-f)**).

3.3. EDS and TEM analysis

From TEM images of the 0.5InVO₄/AgVO₃ nanostructure (**Fig. 3(a)** and (**b**)), it can be clearly observed that the obtained samples were nanorods with spherical crystals. Furthermore, we can observe from HRTEM images that nanostructured composites are formed, as shown in **Fig. 3(c)**. In addition, by measuring the lattice fringes, the resolved interplanar distances were about 0.2986 nm and 0.2687 nm corresponding to the (501) plane of AgVO₃ [33] (0.2992 nm from JCPDS No. 29-1154) and the (112) plane of InVO₄ [40] (0.2708 nm from JCPDS No: 48-0898), respectively. The structure of the 0.5InVO₄/AgVO₃ heterojunctions were also confirmed by the EDS and elemental mapping of the 0.5InVO₄/AgVO₃ sample (**Fig. 3d**). From the images with particular color, the Ag-L, In-L, V-K and O-K elemental maps could be observed, which further demonstrated the existence of InVO₄/AgVO₃ heterojunctions. The result indicated that small particles were the compounds of 0.5InVO₄/AgVO₃.

3.4. The surface elemental compositions

The X-ray photoelectron spectroscopy (XPS) was carried out to investigate the elemental compositions and the valence states of the 0.5InVO₄/AgVO₃ photocatalyst [41]. As shown in **Fig. 4a**, the XPS spectra of the sample were obviously composed of Ag, In, O, and V elements peaks. C 1s XPS spectrum at around 284.8 eV in

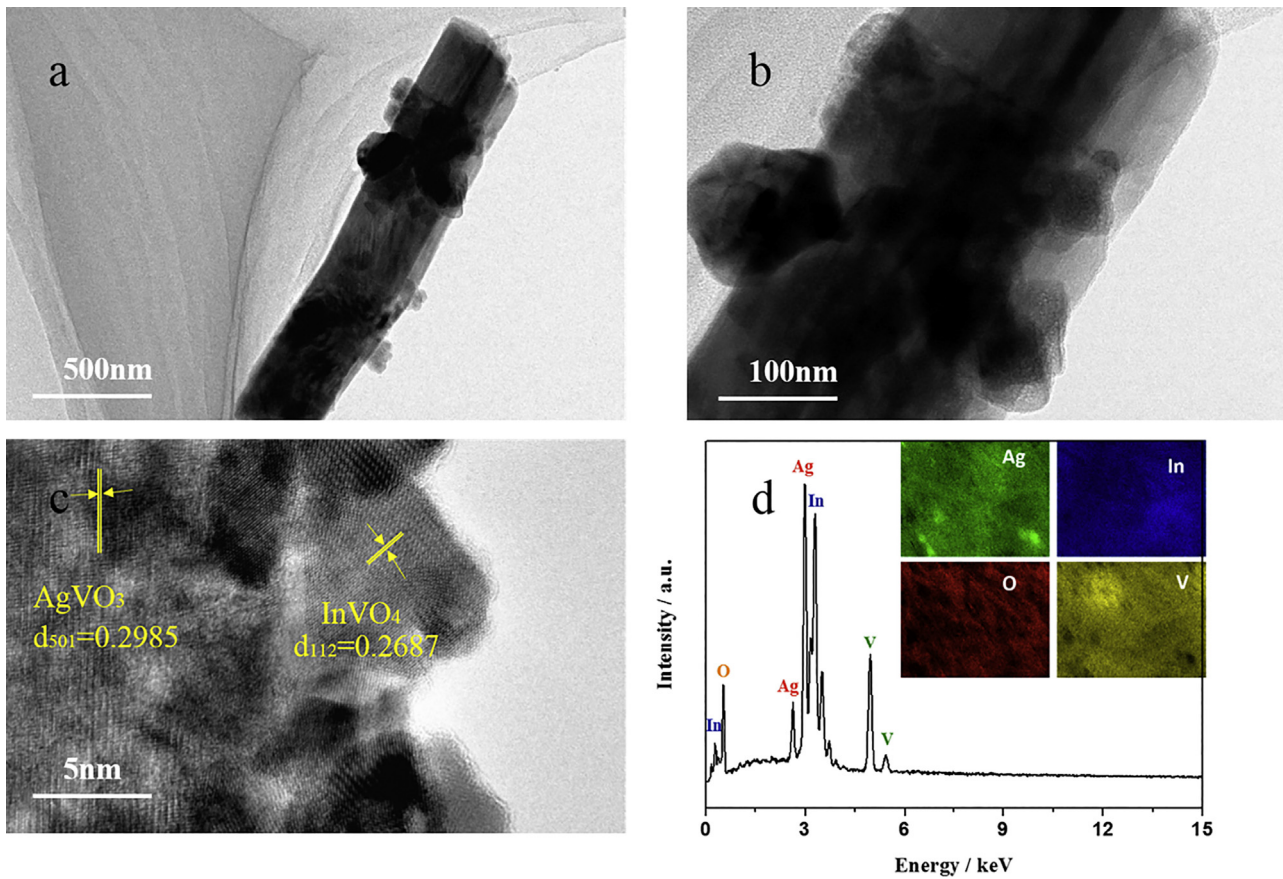


Fig. 3. TEM (a), HRTEM (b), SAED (c) and EDS (d) images of as-synthesized 0.5InVO₄/AgVO₃ compositions.

Fig. 4a is attributed to the signal from hydrocarbon contained in the detection [42]. **Fig. 4b** revealed a typical Ag 3d spectra of this sample, it can be seen that two binding energies could be separated including Ag 3d_{3/2} and Ag 3d_{5/2} at 373.02 eV and 367.02 eV. The spectrum of In 3d (**Fig. 4c**) showed that two peaks at 451.52 eV and 443.92 eV could be attributed to In 3d_{3/2} and In 3d_{5/2} signals of In³⁺ species, respectively, which is in accordance with other XPS result in InVO₄²⁴. The signals of V2p_{1/2} and V2p_{3/2} were observed at approximately 522.97 eV and 515.97 eV, respectively, corresponding to V⁵⁺ in InVO₄ (**Fig. 4d**). In **Fig. 4e**, the O 1s region were fitted with lattice oxygen at about 529.62 eV and absorbed oxygen at 530.82 eV [9,43].

3.5. The photophysical property of the composites

UV-vis diffuse reflectance spectra were measured to study the photophysical property of the InVO₄/AgVO₃ samples. As shown in the DR UV-vis (**Fig. 5A**) of different samples, pure AgVO₃(a) and InVO₄(b) crystals had remarkable absorption at around 650 nm [44] and 430 nm [45] respectively, corresponding to the visible light region. After assembling the InVO₄/AgVO₃ heterojunction, the visible-light response of these samples were greatly improved with red-shifted light absorption, particularly, the 0.5InVO₄/AgVO₃ absorption intensity at around 800 nm was tremendously enhanced as shown in **Fig. 5A(c)**. Furthermore, based on the theory of optical absorption for band gap semiconductors, the band gap energy of pure AgVO₃ and InVO₄ samples can be calculated by the Eq. (1): [3,46]:

$$\alpha h\nu = A(h\nu - E_g)^{n/2} \quad (1)$$

where A, h, ν , and Eg are a constant, Planck constant, the absorption coefficient, the light frequency and band gap energy, respectively. For the value of n, it depends on the type of optical transition of semiconductors (n=1 for direct transition and n=4 for indirect transition) [47]. According to previous literatures, the values of n are 4 and 1 for AgVO₃³³ and InVO₄ [48]. As shown in **Fig. 5B**, the band gap energy of AgVO₃ and InVO₄ crystals were estimated to about 2.4 eV and 2.2 eV, respectively, which were in good agreement with the energy level of structure of pure AgVO₃ and InVO₄ crystals [49].

3.6. The photocatalytic activity

The photocatalytic properties of the InVO₄/AgVO₃ compositions were evaluated by comparing the degradation rate of RhB under visible light irradiation (**Fig. 6a**). According to the results, the blank test presented low degradation of RhB under visible light irradiation, indicating that we could neglect the effect of visible light and other environmental factors. It is shown from the photocatalytic results that the 0.5InVO₄/AgVO₃ photocatalyst was more efficient for the degradation of RhB than the pure AgVO₃, pure InVO₄ and InVO₄/AgVO₃ compositions with other molar ratio. Moreover, as shown in **Fig. 6b**, the maximum absorbance of RhB was at 553 nm [50], and a gradual decrease in the peak intensity at 553 nm was monitored after the application of 0.5InVO₄/AgVO₃ under visible light. After 200 min of irradiation, 99.875% degradation of RhB was achieved. From **Fig. 6c**, there was no obviously changes of photocatalytic efficiency when IPA was added to trap OH[•][51,52]. On the contrary, the degradation of RhB were greatly depressed after MSDS and BQ were injected to trap h⁺ and •O²⁻, which suggested that the

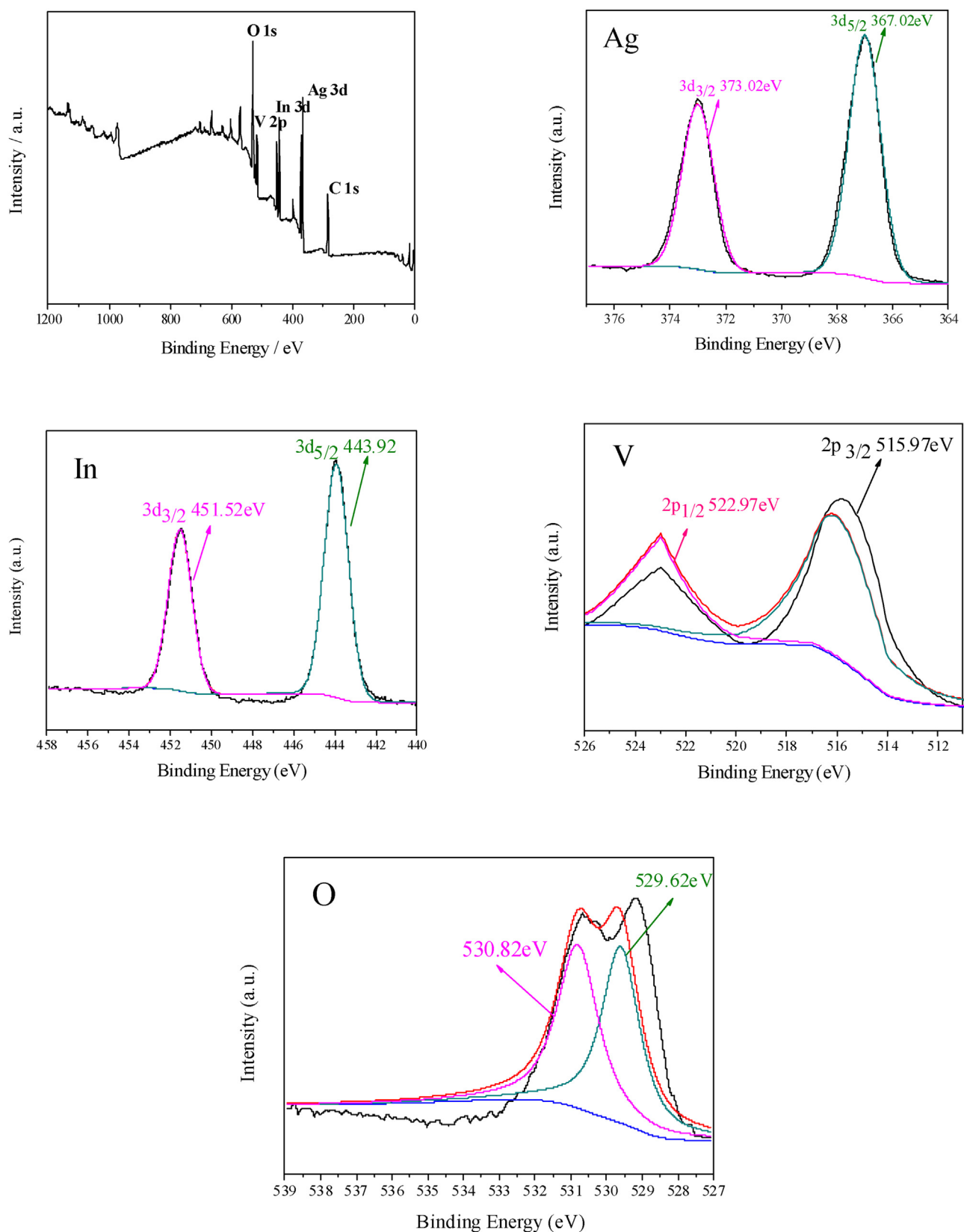


Fig. 4. XPS spectra of $0.5\text{InVO}_4/\text{AgVO}_3$ composition: (a) survey, (b) Ag 3d, (c) In 3d, (d) O 1s, and (e) V 2p.

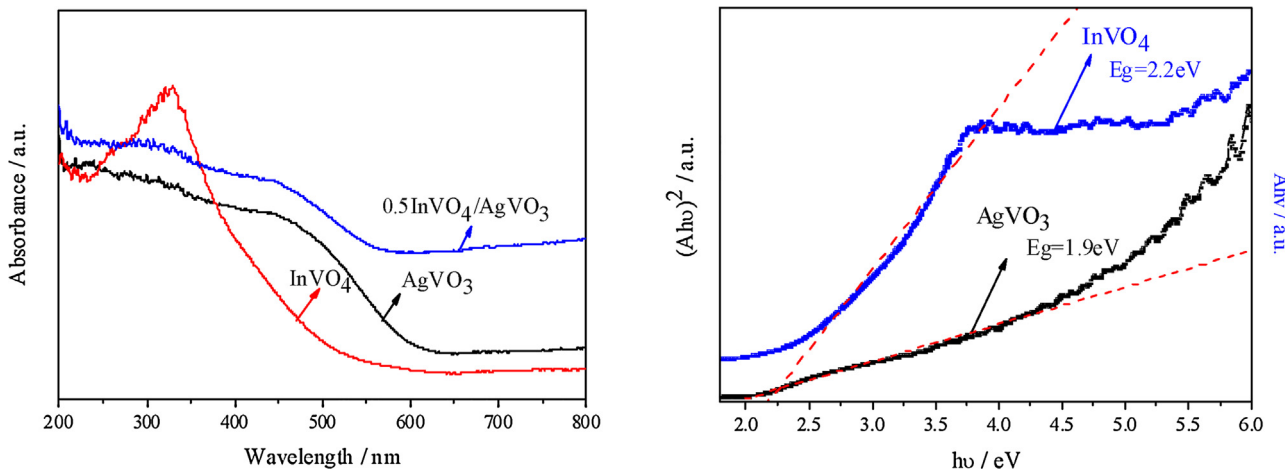


Fig. 5. (A) UV-DRS of (a) AgVO₃, (b) InVO₄, (c) 0.5InVO₄/AgVO₃, (B) Plots of $(\alpha h v)^2$ vs $h v$ for AgVO₃ and InVO₄ crystals.

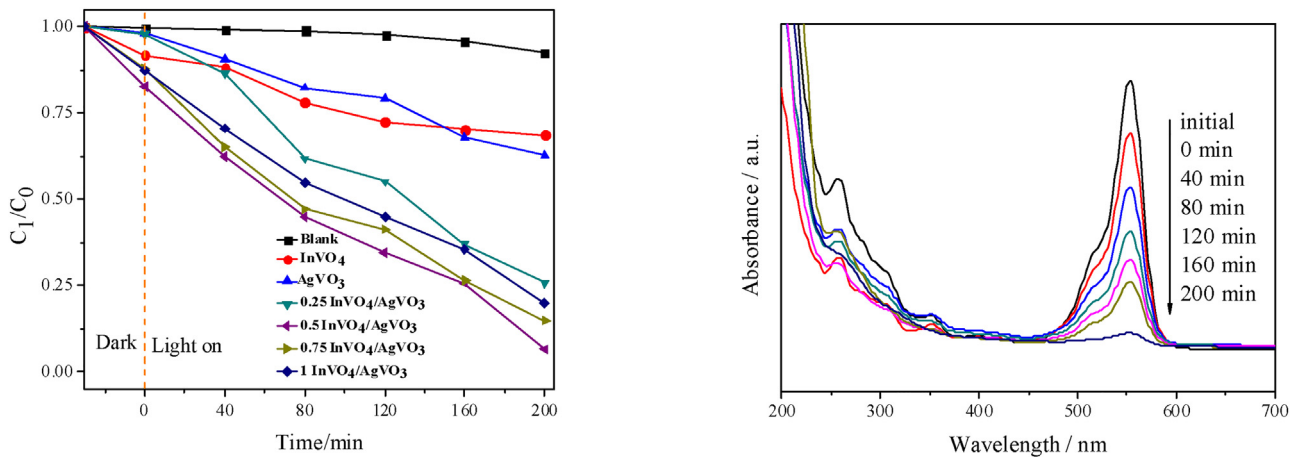


Fig. 6. (a) Degradation efficiencies of InVO₄/AgVO₃ as a function of irradiation time for different photocatalysts (b) UV-DRS of RhB solutions at different time with 0.5InVO₄/AgVO₃ (c) The active species trapping experiments for degradation of RhB with InVO₄/AgVO₃ photocatalyst under visible light irradiation.

•O²⁻ and h⁺ radicals were the major reactive species in the reaction system [33,38].

3.7. Photocatalytic antifouling efficiency

The *E. coli* (6.3×10^6 cfu/mL), *S. aureus* (5.1×10^6 cfu/mL) and *P. aeruginosa* (4.0×10^6 cfu/mL) cells are the representative Gram-negative bacteria, Gram-positive bacteria and marine foul-

ing bacteria. In this paper, three representative bacteria were selected to evaluate the photocatalytic anti-microbial properties of the InVO₄/AgVO₃ compositions under visible light. As shown in Fig. 7(A), the survival curve of *P. aeruginosa* revealed that the quantity of bacteria remained nearly unchanged under visible-light without the addition of photocatalyst, indicating that the effect of the visible light to the bacteria and toxicity of the photocatalyst can be overlooked [53,54]. In addition, the InVO₄/AgVO₃ photocat-

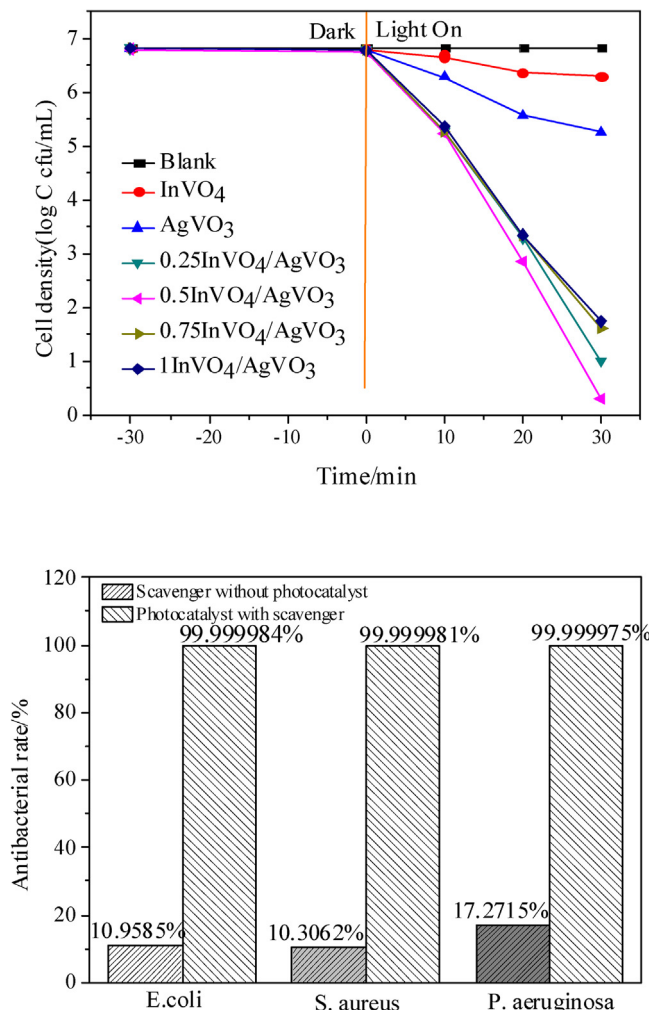


Fig. 7. (a) *E. coli* survival curves with 0.4 mg/mL photocatalyst under visible light, (b) photocatalytic anti-microbial rate histogram of *E. coli*, *S. aureus* and *P. aeruginosa* under visible light with 0.5InVO₄/AgVO₃ for 30 min.

alysts exhibited enhanced photocatalytic anti-microbial activities by comparison with pure InVO₄, pure AgVO₃ and other proportions of InVO₄/AgVO₃ under visible-light. The improved photocatalytic performance of the 0.5InVO₄/AgVO₃ compositions were mainly on account of the formation of p-n heterojunction between InVO₄ and AgVO₃, increasing the valid separation of photo-generated carriers³⁶. As seen in Fig. 7(A), with the increase of InVO₄ mole fraction from 25% to 50%, 0.5InVO₄/AgVO₃ composition presented the most optimum photocatalytic capability, which account for its widest range of visible light from DR UV-vis spectra shown in Fig. 5a. Moreover, it can be seen in Fig. 7(b) that all bacteria were almost killed and the anti-microbial rate of *E. coli*, *S. aureus* and *P. aeruginosa* reached 99.999984%, 99.999951% and 99.999975%, respectively, after 30 min function with 0.5InVO₄/AgVO₃ photocatalyst. Furthermore, the 0.5InVO₄/AgVO₃ composition not only showed an enhanced photocatalytic anti-microbial properties, but also presented a better and broader UV-vis absorption property, making it a perfect photocatalyst in water treatment and marine antifouling, compared to other reported anti-microbial photocatalysts such as TiO₂ [55,56], SiO₂ [57], ZnO [57], Ag/BiOI [58], Bi₂WO₆/BiOI [59] and BiOI/BiVO₄ [36] photocatalyst [60].

In order to observe the destruction of *E. coli* bacterial cells in the photocatalytic process, the appearance of the bacteria were observed by TEM. Fig. 8(a) showed that the wall and plasma membrane of normal *E. coli* bacteria were smooth, while the bacteria

cytoplasm was evenly distributed at the beginning of the photocatalysis. From Fig. 8(b), it could be seen that the cells wall of *E. coli* were broken and damaged. This photograph demonstrated that the destructive process of *E. coli* bacteria was on account of the cell wall attack by the free radical like h⁺ and O²⁻ radicals [34,35,61]. Then the cytochylema penetrated into the periplasmic interval. The cell wall and plasma membrane had lost the ability to maintain the penetration and resist foreign invasion. In addition, Fig. 8(c) also showed that the free radical active species oxidized the left intracellular components completely which made the plasma membrane damaged and dissolved [59,62]. After that, nuclear area disappeared, and cytoplasm and chromosome agglutinated. At last, a typical structure of *E. coli* bacteria in the late stage of the photocatalysis can be observed from Fig. 8(d), the progress by which *E. coli* bacteria were killed and the cell wall were severely damaged, the dissolved membrane, disintegrated nuclear domain, and the disappeared filamentous chromatin can be distinctively observed. By studying the ultrastructural changes of *E. coli*, it can be found that the h⁺ and O²⁻ radicals transfer to the surfaces of bacteria to attack the cells.

3.8. Stability and reusability

To assess the stability and reusability of 0.5InVO₄/AgVO₃ compositions, antifouling experiments for *P. aeruginosa* (4.0*10⁶cfu/mL) were implemented under visible light. After each circulation, the InVO₄/AgVO₃ compositions were separated by centrifuge, washing, and drying in the next cycle. From Fig. 9(a), after eight cycles with similar experiments, the anti-microbial rate of the 0.5InVO₄/AgVO₃ photocatalyst exhibited no significant decrease, which still reaches 99.999%, determining the perfect stability of the composite photocatalyst in photocatalytic antifouling. Moreover, the representative photographs of the *P. aeruginosa* colonies shown in Fig. 9(a) also proved the excellent photocatalytic antibacterial activity of this photocatalyst. Fig. 9(b) was the EDX spectrum of the 0.5InVO₄/AgVO₃ composition after repeating for eight cycles, presented that the chemical composition and crystal structure displayed no significant change after eight cycles with favorable stability of 0.5InVO₄/AgVO₃ photocatalyst.

3.9. Photocatalytic antifouling mechanism

To confirm the primary active species in the antibacterial process, trapping experiments with different scavengers, in which use IPA as an •OH scavenger, DQ as an O²⁻ scavenger, and MSDS as an h⁺ scavenger [51,52], were implemented in the presence of 0.5InVO₄/AgVO₃ photocatalyst under visible light irradiation. As shown in Fig. 10, the antibacterial rate of *P. aeruginosa* reached to 99.9999% after 30 min reaction over 0.5InVO₄/AgVO₃ photocatalyst without any scavenger. Moreover, there was barely impact on the antibacterial performance by the addition of IPA (a scavenger of •OH), implying that •OH was not the main active species in the progress of photocatalytic reaction [63]. However, after DQ and MSDS were added, the antibacterial rates of *P. aeruginosa* were distinctively reduced to 25.48% and 43.79%, respectively. Therefore, O²⁻ and h⁺ free radicals were confirmed as the dominating active species in 0.5InVO₄/AgVO₃ photocatalytic reaction. In addition, the controlling experiments showed that the scavengers have no obviously toxic effect on *P. aeruginosa* antibacterial performance.

To study the improved photocatalytic mechanism of the 0.5InVO₄/AgVO₃ photocatalyst, the band edge positions of conduction band (CB) and valence band (VB) of 0.5InVO₄/AgVO₃ heterojunction can be calculated by the following Eqs. (2), (3):

$$E_{CB} = X - E_C - 0.5E_g \quad (2)$$

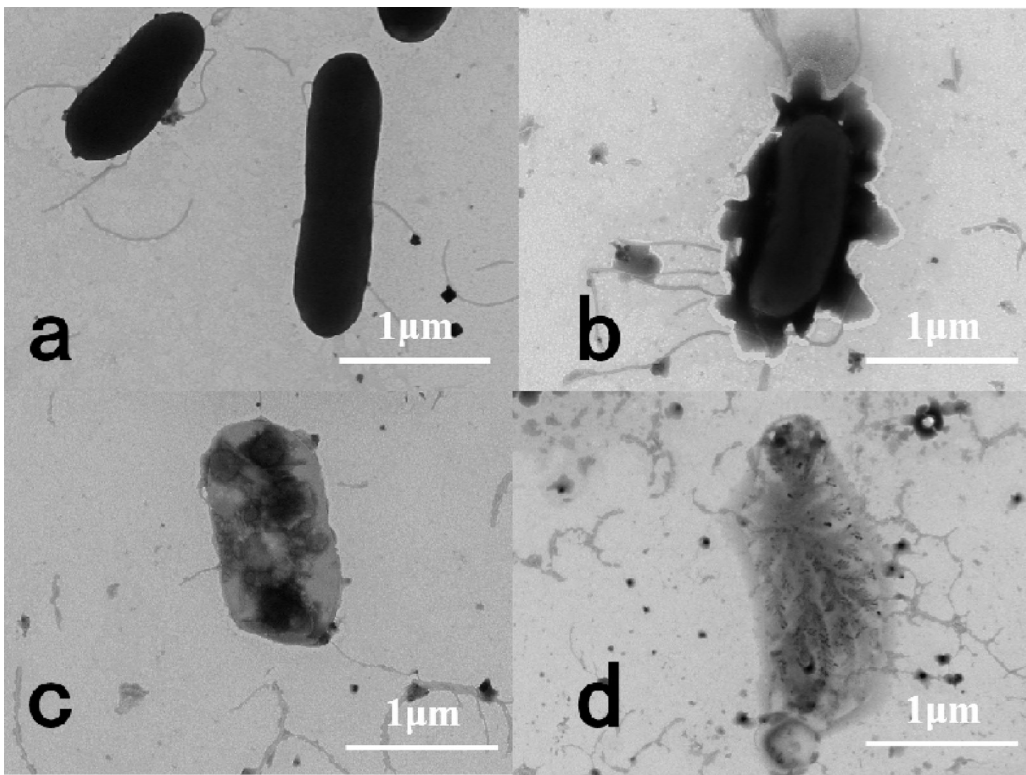
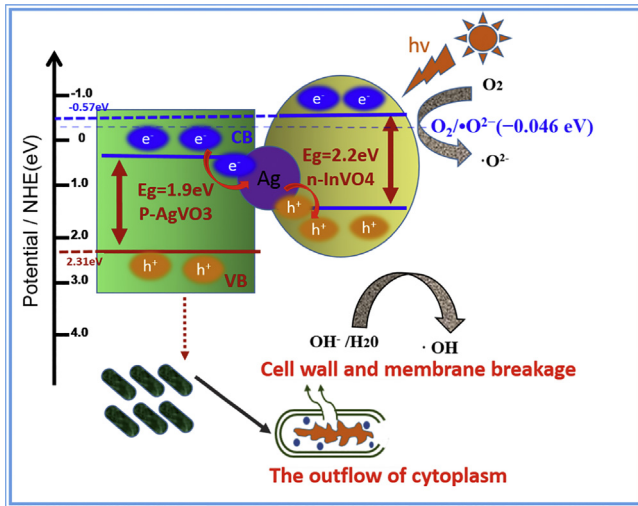


Fig. 8. TEM images of the *P. aeruginosa* cells destruction under visible light irradiation with 0.5InVO₄/AgVO₃.



Scheme 1. Schematic diagram of the proposed mechanism for photo-generated charge carrier transfer in the 0.5InVO₄/AgVO₃ heterojunction under visible-light irradiation.

$$E_{VB} = E_g + E_{CB} \quad (3)$$

where, E_{CB} is the CB edge potential, E_{VB} is the VB edge potential, X is the electronegativity of the semiconductor, which is the electronegativity geometric mean of the constituent atoms (5.86 eV for AgVO₃ [33] and 5.03 eV for InVO₄ [43,64]), E_c is the energy of free electrons on the hydrogen scale (about 4.5 eV), and E_g is the band gap energy of the semiconductor (1.9 eV and 2.2 eV vs NHE for AgVO₃ and InVO₄, respectively [33,38]). According to Eqs. (2) and (3), the CB and VB edge potentials of AgVO₃ are 0.41 eV and 2.31 eV, respectively, and InVO₄ are supposed to be -0.57 eV and 1.63 eV.

As indicated in Scheme 1, the CB of InVO₄ (-0.57 eV) is more cathodic than the standard redox potential of O₂/•O²⁻ (-0.046 eV vs NHE), which exhibited a strong reductive ability. Therefore, according to the trapping experiments and the analysis of redox potentials, it can be concluded that h⁺ and •O²⁻ are the major active free radicals. Nevertheless, the electrons in InVO₄ or the holes in AgVO₃ might rapidly recombine with each other [65]. As shown in previous research, the metal silver would contribute in the separation of electron-hole pairs by the Z-scheme [66–69]. Metal silver could construct a cross-bonding bridge to connect with two semiconductors [70,71]. Firstly, the electrons will transfer from CB potential (0.41 eV) of AgVO₃ into metal silver through the Schottky battier. Secondly, the electrons in metal silver were shifted to the VB of InVO₄ due to the more negative Fermi level of silver than the VB of InVO₄ (1.63 eV), which was faster than the recombination between the electrons in InVO₄ or the holes in AgVO₃. After that, the Z-scheme mechanism was established [72]. As a result, the CB edge potentials of InVO₄ (-0.57 eV) showed the strong reducibility and the VB of AgVO₃ (2.31 eV) possessed a better oxidation capability. Because of the significantly efficient separation of electron-hole pairs by the Z-scheme, 0.5InVO₄/AgVO₃ compositions revealed tremendously enhanced photocatalytic ability.

As shown in Scheme 1, the bacteria were absorbed on the surface of 0.5InVO₄/AgVO₃ heterojunction after connected with these photocatalysts. Then, the h⁺ and •O²⁻ radicals would destroy these cell wall and cytomembrane, which lead to severe cell fracture, the outflow of cytochylema and serious damage of DNA molecules [7,8,62]. Based on the above results and discussion, the photo-induced h⁺ and •O²⁻ free radicals played major roles in the photocatalytic antifouling performance with 0.5InVO₄/AgVO₃ heterojunction.

4. Conclusion

In summary, a novel InVO₄/AgVO₃ heterojunction, a plentiful rod-like structure with spherical shapes, was prepared by an eco-

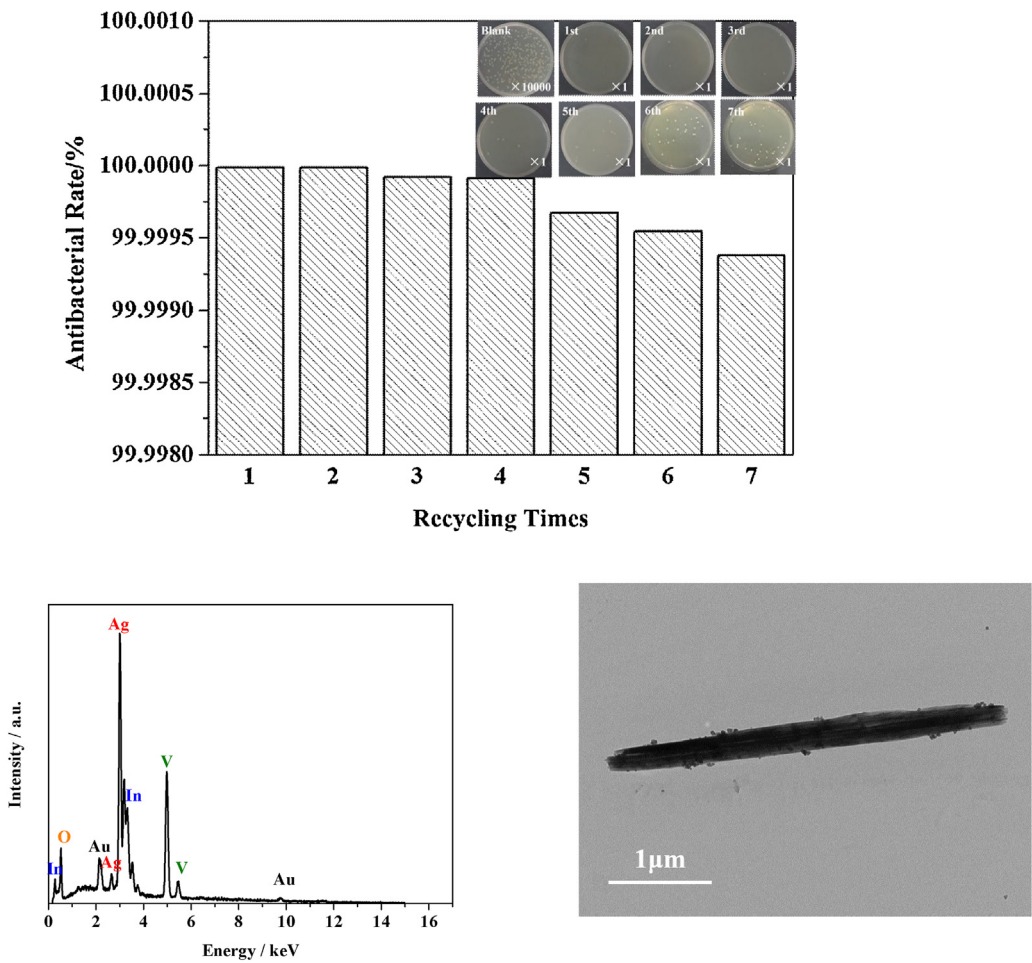


Fig. 9. (a) Recycling anti-microbial tests with *P. aeruginosa* bacteria, photographs of colonies in the antibacterial experiments over 0.5InVO₄/AgVO₃ with *P. aeruginosa* bacteria after eight recycling experiments under visible light irradiation. (b) EDX spectrum, (c) TEM image of 0.5InVO₄/AgVO₃ after eight recycling experiments under visible light irradiation. (c) presents the TEM picture of the 0.5InVO₄/AgVO₃ photocatalyst after eight runs, and it still showed that the nanorods with spherical crystals in accordance with Fig. 2(d). Therefore, these consequences totally showed that the 0.5InVO₄/AgVO₃ composition remained stable and reusable with efficient photocatalytic anti-microbial properties.

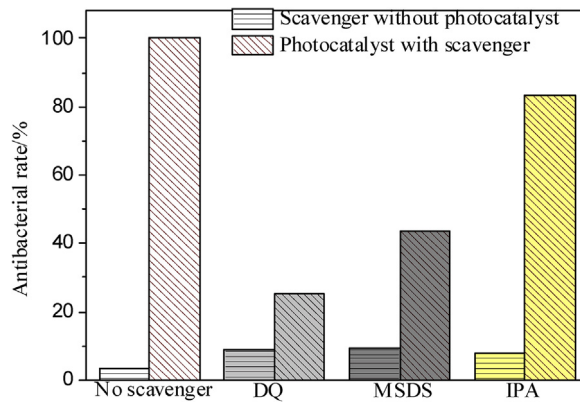


Fig. 10. Effects of scavengers on the photocatalytic antibacterial rate of 0.5InVO₄/AgVO₃ heterojunction for *P. aeruginosa* under visible light irradiation.

nomical and effective method. The compositions and structures of InVO₄/AgVO₃ heterojunctions were identified by XRD, FE-SEM, XPS, TEM and UV-DRS. The InVO₄/AgVO₃ heterojunction showed excellent photocatalytic activities towards the degradation of RhB and the antifouling effects under visible light. In addition, good stability for antibacterial performance of InVO₄/AgVO₃ heterojunction was also affirmed by killing *E. coli*, *S. aureus* and *P. aeruginosa* bacteria after recycling experiments under visible light irradia-

tion. According to the free radicals trapping experiments, h⁺ and •O²⁻ may play the main role in the photocatalytic antifouling performance. Furthermore, a possible photocatalytic antibacterial mechanism was proposed, that the distinctively enhanced photocatalytic performance of the InVO₄/AgVO₃ composition are mainly resulted by the effective separation of electron-hole pairs on the surface of the photocatalyst by the Z-scheme.

Acknowledgements

This work is financially supported by the National Natural Science Foundation of China for Youths (No. 21407065, 21506079), Natural Science Foundation of Shandong Province (No. ZR2016BM08), Natural Science Foundation of Jiangsu Province for Youths (BK20140533), China Postdoctoral Science Foundation (No.: 2014M551520, 2014M560399, 2015T80514), Jiangsu University Scientific Research Funding (No. 14JDG052).

References

- [1] X.T. Wang, J.Z. Duan, J. Zhang, B.R. Hou, *Mater. Lett.* 62 (2008) 1291–1293.
- [2] M. Lejars, A. Margallan, C. Bressy, *Chem. Rev.* 112 (2012) 4347–4390.
- [3] L. Jing, Y. Xu, S. Huang, M. Xie, M. He, H. Xu, H. Li, Q. Zhang, *Appl. Catal. B: Environ.* 199 (2016) 11–22.
- [4] Y.-H. Tseng, D.-S. Sun, W.-S. Wu, H. Chan, M.-S. Syue, H.-C. Ho, H.-H. Chang, *Biochim. et Biophys. Acta (BBA) – Gen. Subj.* 1830 (2013) 3787–3795.
- [5] H. Feng, Y. Li, D. Luo, G. Tan, J. Jiang, H. Yuan, S. Peng, D. Qian, *Chin. J. Catal.* 37 (2016) 855–862.
- [6] I.A. Perales-Martínez, V. Rodríguez-González, S.-W. Lee, S. Obregón, *J. Photochem. Photobiol. A: Chem.* 299 (2015) 152–158.
- [7] O.K. Dalrymple, E. Stefanakos, M.A. Trotz, D.Y. Goswami, *Appl. Catal. B-Environ.* 98 (2010) 27–38.
- [8] A.J. Huh, Y.J. Kwon, *J. Controlled Release* 156 (2011) 128–145.
- [9] J.H. Li, W. Zhao, Y. Guo, Z.B. Wei, M.S. Han, H. He, S.G. Yang, C. Sun, *Appl. Surf. Sci.* 351 (2015) 270–279.
- [10] R. Konta, H. Kato, H. Kobayashi, A. Kudo, *Phys. Chem. Chem. Phys.* 5 (2003) 3061–3065.
- [11] L.T. Denisova, Y.F. Kargin, L.G. Chumilina, V.M. Denisov, *Inorg. Mater.* 52 (2016) 573–577.
- [12] A.S. Vulc, B. Orel, G. Dražić, *J. Solid State Electrochem.* 5 (2001) 437–449.
- [13] L. Ge, M.X. Xu, H.B. Fang, *J. Sol-Gel Sci. Technol.* 40 (2006) 65–73.
- [14] Y. Li, S. Jiang, J. Xiao, Y. Li, *Int. J. Hydrogen Energy* 39 (2014) 731–735.
- [15] Y. Qin, G. Fan, K. Liu, M. Hu, *Sens. Actuators B-Chem.* 190 (2014) 141–148.
- [16] J. Ye, Z. Zou, H. Arakawa, M. Oshikiri, M. Shimoda, A. Matsushita, T. Shishido, *J. Photochem. Photobiol. a-Chem.* 148 (2002) 79–83.
- [17] J. Mao, T. Peng, X. Zhang, K. Li, L. Zan, *Catal. Commun.* 28 (2012) 38–41.
- [18] A. Martirosyan, A. Bazes, Y.-J. Schneider, *Nanotoxicology* 8 (2014) 573–582.
- [19] L. Ge, M. Xu, H. Fang, *Mater. Lett.* 61 (2007) 63–66.
- [20] M. Oshikiri, M. Boero, J. Ye, F. Aryasetiawan, G. Kido, *Thin Solid Films* 445 (2003) 168–174.
- [21] L. Chen, Y. Liu, Z. Lu, D. Zeng, *J. Colloid Interface Sci.* 295 (2006) 440–444.
- [22] Y.H. He, D.Z. Li, Z.X. Chen, Y.B. Chen, X.Z. Fu, *J. Am. Ceram. Soc.* 90 (2007) 3698–3703.
- [23] H. Chang, E.-H. Jo, H.D. Jang, T.-O. Kim, *Mater. Lett.* 92 (2013) 202–205.
- [24] X. Lin, D. Xu, J. Zheng, M. Song, G. Che, Y. Wang, Y. Yang, C. Liu, L. Zhao, L. Chang, *J. Alloys Compd.* 688 (Part B) (2016) 891–898.
- [25] M.W. Shaw, L. Lu, H. Wang, S. Wang, M.L. Zhang, D.D.D. Ma, S.T. Lee, *Chem. Commun.* (2008) 2310–2312.
- [26] P. Rozier, J.M. Savariault, J. Galy, *J. Solid State Chem.* 122 (1996) 303–308.
- [27] R.A. Leising, W.C. Thiebolt, E.S. Takeuchi, *Inorg. Chem.* 33 (1994) 5733–5740.
- [28] E. Deramond, J.M. Savariault, J. Galy, *Acta Crystallogr. Sect. C-Cryst. Struct. Commun.* 50 (1994) 164–166.
- [29] E.S. Takeuchi, W.C. Thiebolt, *J. Electrochem. Soc.* 135 (1988) 2691–2694.
- [30] J. Xie, X. Cao, J. Li, H. Zhan, Y. Xia, Y. Zhou, *Ultrason. Sonochem.* 12 (2005) 289–293.
- [31] X.X. Hu, C. Hu, J.H. Qu, *Mater. Res. Bull.* 43 (2008) 2986–2997.
- [32] X.X. Hu, C. Hu, *J. Solid State Chem.* 180 (2007) 725–732.
- [33] W. Zhao, Z. Wei, H. He, J. Xu, J. Li, S. Yang, C. Sun, *Appl. Catal. A: Gen.* 501 (2015) 74–82.
- [34] M. Yan, Y. Hua, F. Zhu, W. Gu, J. Jiang, H. Shen, W. Shi, *Appl. Catal. B: Environ.* 202 (2017) 518–527.
- [35] A.U. Khan, Q. Yuan, Y. Wei, G.M. Khan, Z.U.H. Khan, S. Khan, F. Ali, K. Tahir, A. Ahmad, F.U. Khan, *J. Photochem. Photobiol., B* 162 (2016) 273–277.
- [36] Z.B. Xiang, Y. Wang, D. Zhang, P. Ju, *J. Ind. Eng. Chem.* 40 (2016) 83–92.
- [37] Z.B. Xiang, Y. Wang, P. Ju, D. Zhang, *Microchim. Acta* 183 (2016) 457–463.
- [38] X. Lin, X. Guo, W. Shi, L. Zhao, Y. Yan, Q. Wang, *J. Alloys Compd.* 635 (2015) 256–264.
- [39] M.R. Parida, C. Vijayan, C.S. Rout, C.S.S. Sandeep, R. Philip, *Appl. Phys. Lett.* (2012) 100.
- [40] J. Chaisorn, K. Wetchakun, S. Phanichphant, N. Wetchakun, *Mater. Lett.* 160 (2015) 75–80.
- [41] G.C. Xiao, X.C. Wang, D.Z. Li, X.Z. Fu, *J. Photochem. Photobiol. a-Chem.* 193 (2008) 213–221.
- [42] H.L. Lin, H.F. Ye, B.Y. Xu, J. Cao, S.F. Chen, *Catal. Commun.* 37 (2013) 55–59.
- [43] U. Lamdad, K. Wetchakun, S. Phanichphant, W. Kangwansupamonkon, N. Wetchakun, *J. Mater. Sci.* 50 (2015) 5788–5798.
- [44] A.Y.S. Malkhasian, *J. Alloys Compd.* 649 (2015) 394–399.
- [45] Y. Yan, X. Liu, W. Fan, P. Lv, W. Shi, *Chem. Eng. J.* 200 (–202) (2012) 310–316.
- [46] S. Thiagarajan, S. Singh, D. Bahadur, *Mater. Chem. Phys.* 173 (2016) 385–394.
- [47] L. Zhang, H. Fu, C. Zhang, Y. Zhu, *J. Solid State Chem.* 179 (2006) 804–811.
- [48] M. Yan, Y. Yan, C. Wang, W. Lu, W.D. Shi, *Mater. Lett.* 121 (2014) 215–218.
- [49] D. Ma, Y.X. Zhang, M.C. Gao, Y.J. Xin, J. Wu, N. Bao, *Appl. Surf. Sci.* 353 (2015) 118–126.
- [50] X. Lin, X. Guo, W. Shi, F. Guo, G. Che, H. Zhai, Y. Yan, Q. Wang, *Catal. Commun.* 71 (2015) 21–27.
- [51] F. Guo, W. Shi, X. Lin, X. Yan, Y. Guo, G. Che, *Sep. Purif. Technol.* 141 (2015) 246–255.
- [52] Y.X. Zhang, D. Ma, J. Wu, Q.Z. Zhang, Y.J. Xin, N. Bao, *Appl. Surf. Sci.* 353 (2015) 1260–1268.
- [53] Z.K. Fang, J.N. Yang, Y. Cao, L.F. Zhu, Q. Zhang, D. Shu, C. He, 2013, in: X. Quan (Ed.), *International Symposium on Environmental Science and Technology*, vol. 18, 2013 (pp. 503–508).
- [54] M. Sokmen, F. Candan, Z. Sumer, *Journal of Photochemistry and Photobiology a-Chemistry* 143 (2001) 241–244.
- [55] P.C. Maness, S. Smolinski, D.M. Blake, Z. Huang, E.J. Wolfrum, W.A. Jacoby, *Appl. Environ. Microbiol.* 65 (1999) 4094–4098.
- [56] J.C. Yu, H.Y. Tang, J.G. Yu, H.C. Chan, L.Z. Zhang, Y.D. Xie, H. Wang, S.P. Wong, *J. Photochem. Photobiol. a-Chem.* 153 (2002) 211–219.
- [57] L.K. Adams, D.Y. Lyon, P.J.J. Alvarez, *Water Res.* 40 (2006) 3527–3532.
- [58] L.F. Zhu, C. He, Y.L. Huang, Z.H. Chen, D.H. Xia, M.H. Su, Y. Xionga, S.Y. Li, D. Shu, *Sep. Purif. Technol.* 91 (2012) 59–66.
- [59] Y.H. Xiang, P. Ju, Y. Wang, Y. Sun, D. Zhang, J.Q. Yu, *Chem. Eng. J.* 288 (2016) 264–275.
- [60] J.C. Shen, H. Yang, Q.H. Shen, Y. Feng, *J. Mater. Sci.* 48 (2013) 7574–7580.
- [61] D. Campoccia, L. Montanaro, C.R. Arciola, *Biomaterials* 34 (2013) 8533–8554.
- [62] P. Ju, Y. Wang, Y. Sun, D. Zhang, *Dalton Trans.* 45 (2016) 4588–4602.
- [63] Y. Long, Y. Wang, D. Zhang, P. Ju, Y. Sun, *J. Colloid Interface Sci.* 481 (2016) 47–56.
- [64] K. Ji, J. Deng, H. Zang, J. Han, H. Arandiyan, H. Dai, *Appl. Catal. B: Environ.* 165 (2015) 285–295.
- [65] C.R. Li, Q.Y. Liu, S.X. Shu, Y. Xie, Y.Q. Zhao, B.Y. Chen, W.J. Dong, *Mater. Lett.* 117 (2014) 234–236.
- [66] Y. Wang, C.G. Niu, L. Zhang, Y. Wang, H. Zhang, D.W. Huang, X.G. Zhang, L. Wang, G.M. Zeng, *RSC Adv.* 6 (2016) 10221–10228.
- [67] R.Y. Xie, L.P. Zhang, H. Xu, Y. Zhong, X.F. Sui, Z.P. Mao, *J. Mol. Catal. A-Chem.* 406 (2015) 194–203.
- [68] H.Y. Li, Y.J. Sun, B. Cai, S.Y. Gan, D.X. Han, L. Niu, T.S. Wu, *Appl. Catal. B-Environ.* 170 (2015) 206–214.
- [69] J.G. Hou, Z. Wang, C. Yang, L. Zhou, S.Q. Jiao, H.M. Zhu, *J. Phys. Chem. C* 117 (2013) 5132–5141.
- [70] M. Xu, L. Han, S.J. Dong, *ACS Appl. Mater. Interfaces* 5 (2013) 12533–12540.
- [71] J.X. Wang, H. Ruan, W.J. Li, D.Z. Li, Y. Hu, J. Chen, Y. Shao, Y. Zheng, *J. Phys. Chem. C* 116 (2012) 13935–13943.
- [72] Y.H. Zhang, Z.R. Tang, X.Z. Fu, Y.J. Xu, *Appl. Catal. B-Environ.* 106 (2011) 445–452.